EurJIC European Journal of Inorganic Chemistry

ChemPubSoc Europe

FULL PAPER

DOI:10.1002/ejic.201201149

Iron(II) Complexes of Two Amine/Imine N_5 Chelate Ligands Containing a 1,4-Diazepane Core – To Crossover or Not To Crossover

CLUSTER ISSUE

Marc Schmidt,[a] Dennis Wiedemann,[a] Boujemaa Moubaraki,[b] Nicholas F. Chilton,[b] Keith S. Murray,[b] Kuduva R. Vignesh,[c] Gopalan Rajaraman,[c] and Andreas Grohmann*[a]

Keywords: Iron / N ligands / Chelates / Magnetic properties / Density functional calculations

Two new chelate ligands, 6-methyl-6-(pyridin-2-yl)-1,4-bis-[(pyridin-2-yl)methyl]-1,4-diazepane (**4a**) and 6-methyl-6-(pyridin-2-yl)-1,4-bis[2-(pyridin-2-yl)ethyl]-1,4-diazepane (**4b**), were synthesized from pyridine-derived precursors in three-step procedures. Both ligands have N_5 donor sets consisting of two tertiary amine and three pyridyl N atoms. Complexation with $FeCl_2$ or $FeBr_2$ in MeOH followed by anion exchange with (nBu$_4$N)PF_6 gave the complexes [Fe(**4a**)X]PF_6 and [Fe(**4b**)X]PF_6 (X = Cl, Br) in moderate-to-good yields. The coordination geometry around the iron(II) centre, as determined by single-crystal X-ray diffraction, is strongly distorted octahedral for ligand **4a** and more regular for ligand **4b**. Magnetic susceptibility measurements show the complexes to contain high-spin iron(II) over the whole range of temperatures ($2 < T < 300$ K). DFT calculations for the complexes of ligands **4a** and **4b** reproduce the high-spin ground state and suggest that exchange of the halide ligand for ligands that exhibit some degree of π-type interaction could induce SCO behaviour. Also, calculations of the zero-field splitting (ZFS) parameters of these complexes rationalize the observed sign change on the basis of different degrees of structural distortion imparted by ligands **4a** and **4b**.

Introduction

Iron, in its coordination compounds, is fascinating for at least two reasons: the ways it interacts with dioxygen and related species,[1,2] and the potential for spin crossover (SCO), especially in the +2 oxidation state.[3,4] Both aspects are combined in haemoglobin, in which O_2 coordination/decoordination induces a change of spin state in the iron ion. Haem and non-haem iron complexes are crucial for dioxygen processing in a multitude of metalloenzymes to bring about substrate oxygenation.[1,2] In this context, we are interested in polypodal N_5 ligands of high symmetry (C_{2v} or C_s), which we have termed "square-pyramidal coordination caps".[5] In (quasi-)octahedral complexes, such ligands leave one coordination site free for the binding of a small monodentate ligand or substrate. Depending on the nature of this ligand, iron(II) complexes undergo temperature-dependent spin crossover[6] or substrate-transforming redox chemistry.[7] Specifically, we attempted to tune the redox potential of iron coordination modules that may be thus obtained by varying the N(amine)/N(imine) ratio of donor atoms in series of such ligands to modify the σ-donor/π-acceptor properties of the ligand or by varying the constraints the ligand imposes on the metal ion, which reflects the concept of the entatic state.[8] Based on these ideas, we recently introduced a ligand containing a hexahydropyrimidine core and gave details of its coordination chemistry with first-row transition metals, including iron.[9] We extend this chemistry in the present contribution and report on the new ligands, 6-methyl-6-(pyridin-2-yl)-1,4-bis-[(pyridin-2-yl)methyl]-1,4-diazepane (**4a**) and 6-methyl-6-(pyridin-2-yl)-1,4-bis[2-(pyridin-2-yl)ethyl]-1,4-diazepane (**4b**), and their chlorido- and bromidoiron(II) complexes. The ligands vary in the number of methylene groups (one vs. two) joining the tertiary amine N atoms to their pyridyl substituents and are, therefore, expected to induce different degrees of coordinative strain upon complexation. The characterization includes variable-temperature magnetic data for both types of complex (Fe^{II}/**4a**, Fe^{II}/**4b**), as well as a theoretical study of different spin-state structures and energies (Fe^{II}/**4b**). This study has also been extended to the hypothetical (thiocyanato-κ*N*)iron(II) complexes of both ligands, which are not yet synthetically accessible, to assess their expected temperature-dependent spin behaviour.

[a] Institut für Chemie, Technische Universität Berlin, Straße des 17. Juni 135, 10623 Berlin, Germany
Homepage: http://www.bioanorganik.tu-berlin.de/
[b] School of Chemistry, Monash University, Building 23, Clayton, Victoria 3800, Australia
[c] Department of Chemistry, Indian Institute of Technology Bombay, Powai, Mumbai 400076, India

Supporting information for this article is available on the WWW under http://dx.doi.org/10.1002/ejic.201201149.

Results and Discussion

Ligand Synthesis

The synthesis of ligands **4a** and **4b** proceeds in three steps (Scheme 1) with ditosylate **1** as the starting material.[10] The generation of **3** from **1** requires the formal introduction of 1,2-ethylenediamine (en) by nucleophilic substitution. When this is attempted directly, the reaction is unspecific and proceeds, at least in part, with the intermolecular coupling of **1**. This may be avoided by protecting the NH_2 functions in 1,2-ethylenediamine with *p*-toluenesulfonyl chloride (TsCl).[11] Upon deprotonation of the tosylamine groups with NaH or NaOH in tetrahydrofuran (THF), **1** is added as a solid and the reaction mixture is subsequently heated to reflux for several days. The suspension gradually turns brown, and ESI mass spectrometry is compatible with a mixture of **2** and **2a** (**2a** is the monosubstituted side product.)

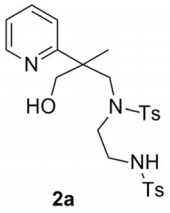

2a

Overall, as judged by regular probing of the mixture with ESI-MS, the reaction of **1** is sluggish, most likely because of the limited solubility of the starting materials in THF. Therefore, we decided to suspend the ethylenediamine ditosylate in water and react it with solid NaOH at 100 °C. In the course of one hour, this produces a colourless solution, in which we assume the RNHTs groups to be fully deprotonated. The boiling was allowed to subside, and a warm solution of **1** in toluene was added in one portion to produce a two-phase system, which was then stirred vigorously and heated to reflux for two days. ESI-MS of the organic phase indicated complete disappearance of **1** (if the two-phase system is not stirred with sufficient vigour, the rate of the reaction is slowed drastically). The new solvent system has major advantages: (a) increased reaction rate and yield of **2** (> 80%) when compared with the reaction in THF (several weeks, after which < 30% of **1** had reacted); (b) the ditosylate **1** is practically insoluble in H_2O, which minimizes the formation of **2a**; (c) simple workup to obtain **2** sufficiently pure for the subsequent synthetic step (see Exp. Sect.). The tosyl groups were cleaved by dissolving **2** in concentrated H_2SO_4 and stirring the reaction mixture at 130 °C for 14 h.[12] 6-Methyl-6-(pyridin-2-yl)-1,4-diazepane (**3**) was then used without further purification and reacted with 2-(chloromethyl)pyridine and potassium carbonate in acetonitrile[13] or 2-vinylpyridine and acetic acid in MeOH[14] to give the N_5 chelate ligands **4a** and **4b**, respectively. The crude ligands are obtained as yellow-red oils, which can be purified by repeated washing with hexane. Compounds **4a** and **4b** are yellow oils (correct elemental analyses), and the yields are 63% and 42%, respectively (over three steps, based on **1**).

Iron(II) Complexes

The formation of iron(II) complexes of ligands **4a** and **4b** by using $FeCl_2$ or $FeBr_2$ in methanol is straightforward. The bromide salt [Fe(**4b**)Br]Br (**5**) was precipitated from solution as an amorphous solid by the addition of diethyl ether. Solid $(n\text{Bu}_4\text{N})PF_6$ was added to the MeOH solutions to precipitate polycrystalline material (yellow in all cases), and the chlorido and bromido complexes [Fe(**4a**)Cl]PF_6 (**6**), [Fe(**4a**)Br]PF_6 (**7**), [Fe(**4b**)Cl]PF_6 (**8**) and [Fe(**4b**)Br]PF_6 (**9**) were thus obtained (cf. Exp. Sect.). Single crystals were grown by recrystallization from acetonitrile. X-ray analyses reveal isomorphous pairs (**6** and **7**, **8** and **9**). All complexes are acetonitrile solvates in their single crystals and contain one solvent molecule (**6**/**7**) or half a solvent molecule (**8**/**9**). Representative cation structures are shown in Figure 1, and the crystallographic data is given in Table 6.

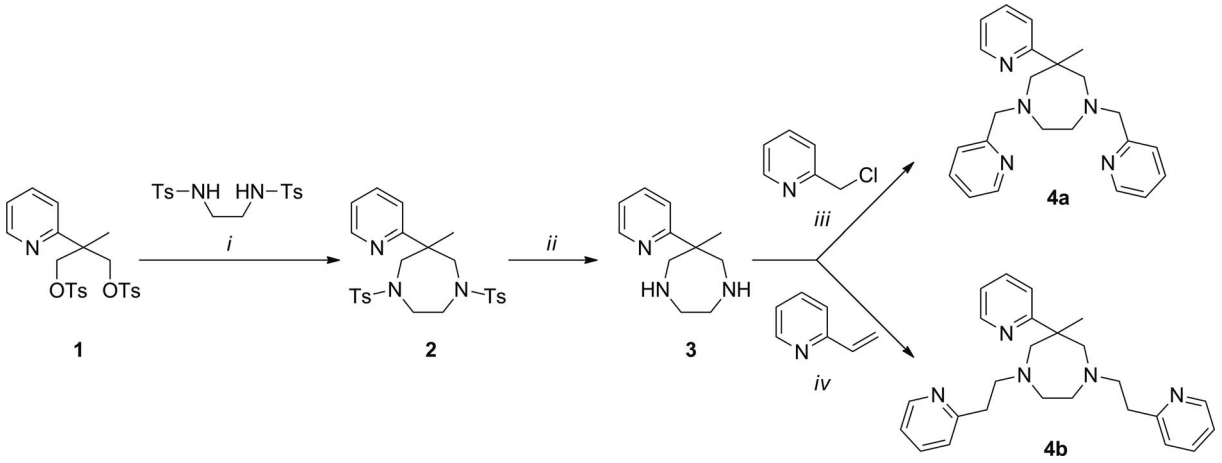

Scheme 1. Synthesis of the N_5 ligands **4a** and **4b**: i) NaOH, water/toluene (50:50), reflux, 2 d; ii) H_2SO_4, 130 °C, 1 d; iii) MeCN, K_2CO_3, 55 °C, 3 d; iv) MeOH, acetic acid, reflux, 2 d.

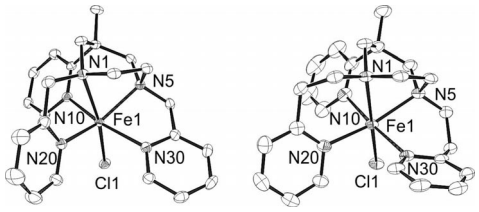

Figure 1. Structures of the cations in **6** (left) and **8** (right). ORTEP representations with ellipsoids at the 50% probability level; hydrogen atoms, hexafluorophosphate counterions and acetonitrile molecules omitted for clarity.

The bond lengths in both types of complex are unexceptional, and the average Fe–N bond length of ca. 2.2 Å indicates high-spin iron(II) in all cases at 150(1) K (Table 1).[15,16] The halide ligand X1 (X = Cl or Br) is *trans* to a tertiary amine N atom (N1) in all structures, although, at least for complexes of ligand **4b**, a *trans* arrangement N10–Fe1–X1 would not appear precluded by structural constraints. Indeed, structural data to be published elsewhere show that ligand exchange [(chloride→triflate (OTf)] leads to a *trans* arrangement (N10–Fe1–OTf) in the triflatoiron(II) complex of ligand **4b**. The coordination environment in **6** and **7**, in which ligand **4a** provides a more constricted N_5 donor set, is severely distorted from (quasi-)octahedral, whereas it is more regular in **8** and **9**, in which the ligand tethers are longer (ligand **4b**). We have evaluated this distortion by using the "Continuous Symmetry Measures" proposed by Zabrodsky, Peleg and Avnir, which "quantify the minimal distance movement that the points of an object have to undergo in order to be transformed into a shape of the desired symmetry."[17,18] The parameter $S(O_h)$, which ideally is zero, is greater than five for **6/7** and lies between one and two for **8/9**, as is expected for unstrained HS iron(II) compounds (Table 1). The average Fe–N bond length does not vary strongly between the complexes, and the deformation parameter Σ, which is a measure of the deviation of all *cis* angles from 90°, reflects this behaviour exactly; for the heavily distorted complexes **6** and **7**, it has high values of ca. 145°.

Table 1. Coordinative bond lengths [Å], *cis* angles [°] and distortion parameters Σ and $S(O_h)$ for complexes **6**–**9**.

	6 (X = Cl)	**7** (X = Br)	**8** (X = Cl)	**9** (X = Br)
Fe1–N1	2.3373(17)	2.311(3)	2.298(2)	2.281(3)
Fe1–N5	2.1878(17)	2.187(3)	2.238(2)	2.229(3)
Fe1–N10	2.1625(18)	2.159(3)	2.206(2)	2.204(3)
Fe1–N20	2.1317(18)	2.134(3)	2.211(2)	2.209(3)
Fe1–N30	2.2633(18)	2.259(3)	2.250(2)	2.243(3)
Fe1–X1	2.3738(6)	2.5397(6)	2.4135(7)	2.5959(6)
d_{FeN}	**2.217(4)**	**2.210(7)**	**2.241(4)**	**2.233(7)**
N1–Fe1–N5	71.15(6)	71.70(11)	71.99(8)	72.27(11)
N1–Fe1–N10	79.03(6)	79.74(11)	84.62(8)	84.91(11)
N1–Fe1–N20	75.81(6)	76.30(11)	88.51(8)	89.81(11)
N1–Fe1–N30	107.16(6)	107.37(11)	95.68(7)	96.24(11)
X1–Fe1–N5	114.12(5)	112.17(8)	104.37(6)	102.98(8)
X1–Fe1–N10	88.58(5)	88.47(8)	86.58(6)	86.00(9)
X1–Fe1–N20	103.33(5)	104.06(9)	96.19(6)	96.09(8)
X1–Fe1–N30	85.67(5)	84.55(8)	92.69(5)	92.34(8)
N5–Fe1–N10	96.90(7)	97.24(11)	93.64(8)	94.37(12)
N5–Fe1–N30	73.01(6)	72.96(11)	81.46(7)	81.31(11)
N10–Fe1–N20	99.61(7)	99.79(11)	92.79(9)	92.46(13)
N20–Fe1–N30	95.19(7)	95.18(11)	92.49(8)	92.50(12)
Σ/°[a]	143.1(2)	142.1(4)	74.7(3)	72.7(4)
$S(O_h)$[b]	5.09	5.21	1.55	1.81

[a] $\Sigma = \sum_{i=1}^{12} |90 - \phi_i|$; ϕ_i: angles L^a–Fe–L^b between *cis*-positioned Fe–L bonds.[19] [b] See text.

Magnetic Susceptibilities

Plots of $\chi_M T$ vs. T for the mononuclear iron(II) complexes **6** and **7** are similar in shape and that for **6** is shown in Figure 2 (top; see Supporting Information for plots of **7**). The $\chi_M T$ values remain independent of temperature between 300 and ca. 50 K with values of 3.45 (μ_{eff} = 5.25μ_B) and 3.5 $cm^3 mol^{-1} K$ (μ_{eff} = 5.29μ_B) for **6** and **7**, respectively, which are typical of high-spin distorted octahedral Fe^{II} compounds. A rapid decrease in $\chi_M T$ then occurs and it reaches 2.67 (μ_{eff} = 4.62μ_B) and 1.63 $cm^3 mol^{-1} K$ (μ_{eff} = 3.61μ_B), respectively, which is indicative of zero-field splitting of ground $^5A_{1g}$ states. The magnetization isotherms, M vs. H, at temperatures 2 to 20 K, are shown in Figure 2 (bottom) and do not exhibit saturation even at the lowest temperature (2 K) and highest field (5 T), at which the M values of 3.04 and 2.75 $N_A\mu_B$ are much less than the S = 2 value (4.90μ_B) because of zero-field splitting caused by spin–orbit coupling effects. The susceptibility and magnetization data for **6** and **7** were simultaneously fitted to the axial spin Hamiltonian $\hat{H} = D(\hat{S}_z^2 - \frac{1}{3}\hat{S}^2) + \mu_B g\hat{S} \cdot B$ with S = 2 by use of program *PHI*[20] (Figure 2 and Figure S1 in the Supporting Information). The best-fit parameters were determined to be as given in Table 2.

The plots of $\chi_M T$ vs. T for **8** and **9** are again similar in shape. Figure 3 (top) shows the plots for **8** (see Supporting Information for plots of **9**). Similar to the behaviour of complexes **6** and **7**, the $\chi_M T$ values remain independent of temperature between 300 and ca. 50 K and are 3.25 $cm^3 mol^{-1} K$ (μ_{eff} = 5.10 μ_B) as expected for high-spin distorted octahedral Fe^{II}. There is a subsequent rapid decrease in $\chi_M T$ and it reaches 1.2 $cm^3 mol^{-1} K$ (μ_{eff} = 3.10 μ_B), which again indicates zero-field splitting of ground $^5A_{1g}$ states. The magnetization isotherms, M vs. H at temperatures 2 to 20 K are shown in Figure 3 (bottom). As for **6** and **7**, saturation is not reached even at the lowest temperature (2 K) and highest field (5 T), at which the M value of 2.7 $N_A\mu_B$ is much less than the S = 2 value because of zero-field splitting caused by spin–orbit coupling effects. The best-fit parameters (for the susceptibility and magnetization data; simultaneous fit to the same axial spin Hamiltonian as for **6** and **7**; Figures 3 and S2) were determined to be as given in Table 2.

Although further applied-field Mössbauer and EPR spectroscopy (parallel mode)[21] would be required to confirm the change in sign of D between the complexes of ligands **4a** and **4b**, the simultaneous fitting of susceptibilities and magnetizations involved a wide exploration of param-

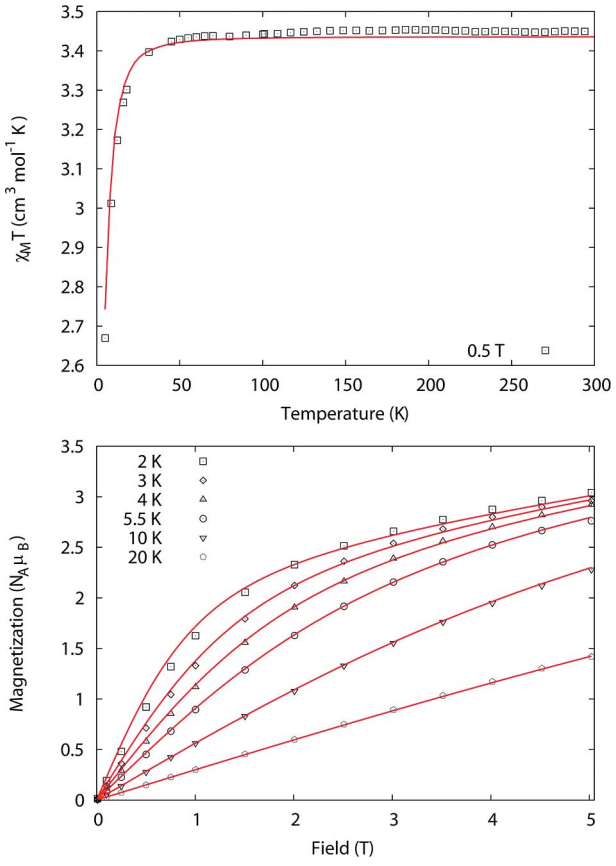

Figure 2. Plot of $\chi_M T$ vs. T for **6** in a field of 0.5 T (top). Magnetization isotherms for **6** at temperatures 2, 3, 4, 5.5, 10 and 20 K (bottom). The red lines are the best fits calculated by using the parameters given in the text.

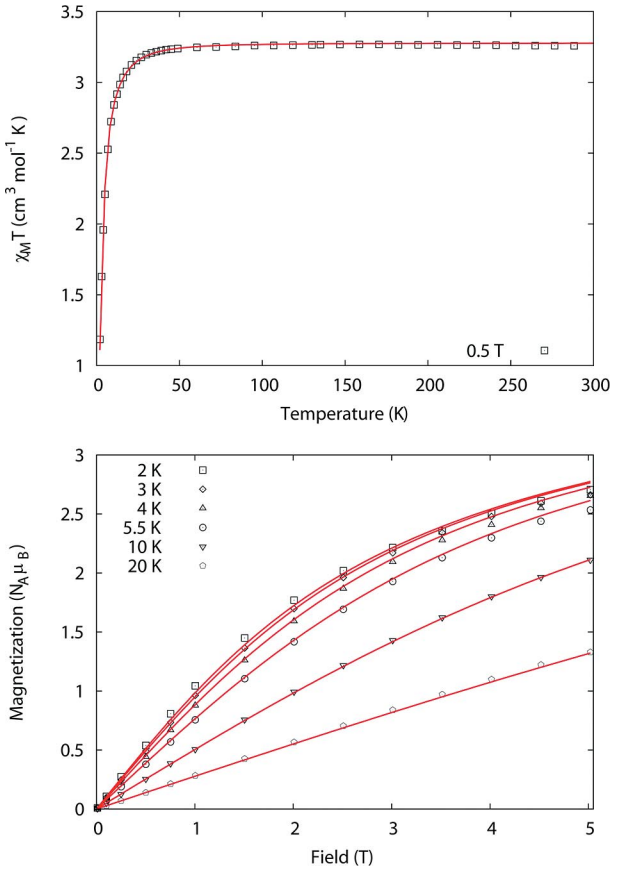

Figure 3. Plot of $\chi_M T$ vs. T for **8** in a field of 0.5 T (top). Magnetization isotherms for **8** at temperatures 2, 3, 4, 5.5, 10 and 20 K (bottom). The red lines are the best fits calculated by using the parameters given in the text.

Table 2. Best-fit parameters for the susceptibility and magnetization data obtained for complexes **6**–**9**.

	g	D [cm^{-1}]
[Fe(**4a**)Cl]PF_6 (**6**)	2.14	–4.50
[Fe(**4a**)Br]PF_6 (**7**)	2.17	–7.48
[Fe(**4b**)Cl]PF_6 (**8**)	2.09	7.81
[Fe(**4b**)Br]PF_6 (**9**)	2.14	13.2

eter space and we are confident of the difference in sign in D. The origin of this sign change, in a parameter that relates to second order spin–orbit coupling and to distortions from octahedral symmetry, presumably relates to the distortions discussed in the crystallographic section and expressed as $S(O_h)$ and Σ, which are markedly different for the two ligand systems (Table 1). Interestingly, whereas the metal–ligand bond lengths in d^4 Mn^{III} Jahn–Teller distorted octahedral species can be related to the sign of D (negative for axial elongation),[22] this is not evident in the present structures. The presence of the "hetero" ligand, Cl or Br, might play a role here. An experiment worth pursuing on the negative D complexes **6** and **7** is to measure their in-phase and out-of-phase AC susceptibilities at low temperature to check for slow relaxation of magnetization [i.e., single molecule magnetism, (SMM)], a feature recently observed in distorted Fe^{II} compounds with negative D values[23] and for which theoretical calculations of the influence of ligand distortions upon D and E (rhombic) values have been given.[24]

Theoretical Studies

Theoretical studies have been undertaken to unfold the spin-crossover features, if any, observed in the monomeric complexes **6**–**9**. We acknowledge that DFT calculations, per se, relate to species in the gaseous phase and thus do not include crystalline/solvent/packing effects; nevertheless, they are useful for probing spin states and spin transitions and also to underpin the electronic structure of the complex of interest. Here, calculations have been performed with the hybrid functional B3LYP, which tends to favour the HS state. Exchange-correlation functionals incorporating less (< 20%) exact exchange, or double-hybrid functionals incorporating correlation from MP2 methods, have been found to be superior to B3LYP calculations.[25–28] Despite these known issues, B3LYP in general gives structures that are in good agreement with X-ray structure determinations and is the functional of choice for the computation of spectroscopic parameters.

Different spin-state structures and energies were computed to understand the spin-crossover features, g and zero-

Table 3. Selected structural parameters computed by using the B3LYP functional (see Figure 4 for labels).

Structural parameter	6				7				8				9			
	X-ray	HS	IS	LS	X-ray	HS	IS	LS	X-ray	HS	IS	LS	X-ray	HS	IS	LS
Fe–N1	2.188	2.233	2.157	2.097	2.187	2.232	2.157	2.101	2.299	2.344	2.384	2.127	2.281	2.348	2.396	2.129
Fe–N2	2.338	2.359	2.435	2.064	2.311	2.355	2.434	2.069	2.238	2.303	2.204	2.109	2.229	2.295	2.195	2.115
Fe–N3	2.163	2.207	2.010	2.024	2.159	2.211	2.012	2.028	2.250	2.292	2.058	2.088	2.205	2.289	2.061	2.053
Fe–N4	2.263	2.342	2.060	2.086	2.259	2.346	2.062	2.088	2.206	2.224	2.026	2.046	2.243	2.229	2.030	2.092
Fe–N5	2.132	2.160	2.118	1.984	2.139	2.161	2.113	1.994	2.212	2.247	2.206	2.064	2.209	2.251	2.194	2.070
Fe–Cl	2.374	2.376	2.423	2.420	–	–	–	–	2.413	2.425	2.492	2.450	–	–	–	–
Fe–Br	–	–	–	–	2.540	2.553	2.613	2.611	–	–	–	–	2.596	2.586	2.670	2.616
Cl–Fe–N2	167.2	170.6	171.7	173.4	–	–	–	–	170.2	171.2	172.6	169.9	–	–	–	–
Br–Fe–N2	–	–	–	–	168.1	171.2	170.6	172.6	–	–	–	–	169.4	170.3	170.9	169.3
N5–Fe–N1	139.2	139.6	142.0	158.1	140.2	139.3	142.0	157.4	158.7	159.1	160.8	170.6	160.1	158.9	160.9	170.1
N3–Fe–N4	165.0	161.9	168.6	165.3	164.6	163.8	169.2	166.0	174.7	173.9	176.4	172.9	174.9	175.1	177.2	173.5

field splitting (zfs; D) parameters to complement the experimental data. The computed structural parameters for **6**–**9** along with X-ray structural parameters are summarized in Table 3. The structural parameters of the optimized structures are in general in good agreement with the X-ray structural parameters, and the short and long bonds observed within the distorted octahedron are nicely reproduced by theory. The high-spin (S = 2) structure in particular resembles the X-ray structure very closely.

The optimized structures (ground-state structures) of **6** and **9** along with computed energies for **6**–**9** are shown in Figure 4. For all four complexes, the high-spin (HS) state is found to be the ground state; this is consistent with the experimental observations. In addition, the low-spin (LS) states lie at 54.3, 54.6, 50.7 and 52.3 kJ mol^{-1} for **6**, **7**, **8** and **9**, respectively. The intermediate-spin (IS) states lie much higher in energy. As structural optimizations have been performed, the entropy change between the ground state HS and LS spin states, $\Delta S = S_{HS} - S_{LS}$, has also been estimated and this is found to be 57.7, 59.6, 57.6 and 60.4 J mol^{-1} K^{-1}, and the enthalpy change is computed to be –58.0, –59.0, –55.3 and –57.4 kJ mol^{-1} for **6**, **7**, **8** and **9**, respectively. These estimated energy gaps are consistent with the experimental reports for Fe^{II} spin crossover compounds.[29–31]

As spin crossover depends on enthalpy and entropy contributions, spin-state splitting and the corresponding free-energy change essentially determines the temperature at which the SCO transition is observed. The plot and energies of d-based orbitals of **6** and **8** are shown in Figure 5. The energy gap between the t_{2g}-like and e_g-like orbitals for **8** and **9** is nearly 128 kJ mol^{-1}, whereas for **6** and **7** it is nearly 300 kJ mol^{-1}. This splitting energy clearly illustrates that ligand-induced structural changes significantly alter the energy levels and hence the properties of the complexes (see below). The generation of the low-spin complex demands pairing of electrons in the d_{xz} and d_{yz} orbitals and both orbitals are strongly influenced by halogenido coordination (Figure 5). This supports the notion that the SCO feature can be tuned by axial ligation and ligands exhibiting mod-

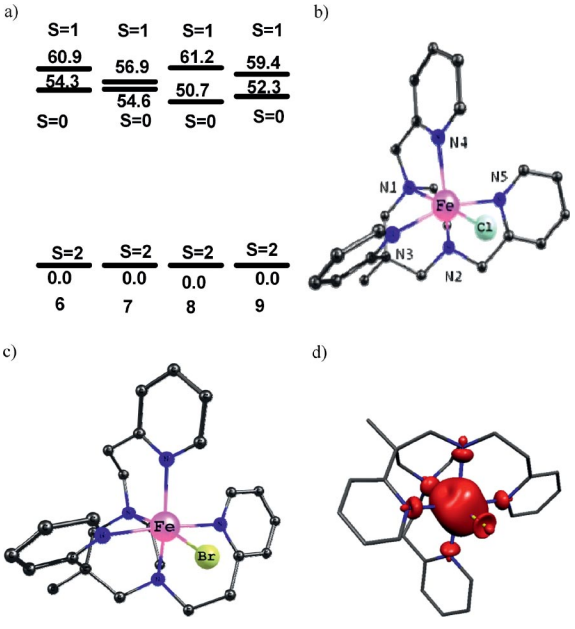

Figure 4. (a) Energy level gaps [kJ mol^{-1}] computed for different electronic configurations in **6**–**9**. Optimized ground state structure of (b) **6** and (c) **9**. (d) Spin density plot for **8**.

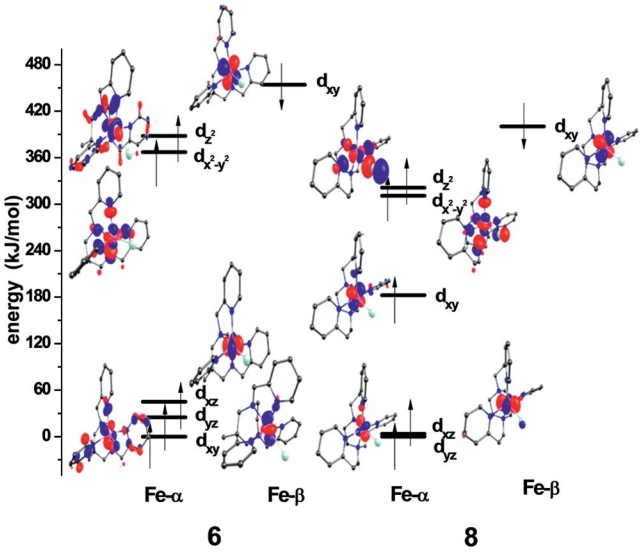

Figure 5. Eigenvalue plot computed for **6** and **8**. Here, α and β represent spin-up and spin-down configurations. The energies are scaled to the lowest spin-up orbitals in each case. For orbital labelling, the Fe–Cl bond direction has been defined as the z axis and one of the equatorial Fe–N(imine) directions as the x axis.

erate-to-weak π-type interactions are ideal for the observation of SCO features. In this context, we have modelled axial thiocyanato ligation in place of Br ligation in **9**.[32] As expected, the HS–LS gap is reduced to 38.6 kJ mol^{-1}; however, this gap is likely still too large for the observation of SCO (see Figure S3 for the optimized structure and computed energy gap). A HS–LS gap of –25 to 0 kJ mol^{-1} is suggested as an ideal gap for the observation of SCO by Neese et al.[26] This situation should be compared with the results obtained for a related N_5 ligand L, 2,2′-(pyridine-2,6-diyl)bis(2-methylpropane-1,3-diamine).[6] Whereas the bromido complex [Fe^{II}BrL]Br is high spin (four unpaired electrons) at room temperature, the carbonyl complex [Fe^{II}(CO)L]Br$_2$ is low spin and diamagnetic,[7] and [Fe^{II}L(NMe-imidazole)](OTf)$_2$ shows SCO above 300 K.[6] In this context, for mononuclear iron(II) complexes to be bistable (i.e., show temperature-dependent SCO behaviour) the ligand sphere usually consists of six N donors (mainly N heterocycles),[33] but N_4O_2 donor sets are also known.[34]

DFT-computed isotropic *g* values for **6**–**9** are given in Table 4 along with computed ZFS parameters. The computed *g* tensors are nearly isotropic. Compared to the experimental values, the *g* tensors are slightly underestimated. Although the computed ZFS parameters are severely underestimated compared to the experimental values, the calculations reproduce the negative and positive sign of *D* observed with ligands **4a** and **4b**, respectively. The fact that the ZFS parameter is underestimated by DFT is due to neglect of contributions from the triplet and singlet states; this is well-documented in the literature.[35,36] The different contributions to the net *D* parameter are summarized in Table 5. It is clear that D_{soc} (spin–orbit) makes a significant contribution and its sign changes as we move from complexes **6**/**7** to **8**/**9**. Similar behaviour is noted also for D_{SS} (spin–spin) contributions. The largest contributions to D_{soc} arise from DOMO (doubly-occupied molecular orbital) to SOMO (singly-occupied MO) β→β excitations and SOMO to SOMO α→β excitations. The sign change occurs because of the difference in the energetics of the d orbitals between the two ligands sets. The intricate differences in the d-orbital energies between **6** and **8** are shown in Figure 5. Most importantly, the d_{xy} orbital energy is significantly high in complex **8**; this leads to small d_{xy}–$d_{x^2-y^2}$ (α→β) transition energies and this, in turn, leads to a sign change between **6** and **8** for the ZFS parameter. Notably, for a Jahn–Teller compressed {Mn^{III}Cu^{II}} complex, such orbital mixing leads to a positive ZFS parameter.[37]

Table 4. B3LYP-computed *g*, *D* and *E*/*D* values for **6**–**9**.

Complex	*D* [cm^{-1}]	*E*/*D*	*g* (isotropic)
[Fe(**4a**)Cl]PF$_6$ (**6**)	–2.280	0.286	2.006
[Fe(**4a**)Br]PF$_6$ (**7**)	–1.026	0.066	2.006
[Fe(**4b**)Cl]PF$_6$ (**8**)	2.587	0.315	2.046
[Fe(**4b**)Br]PF$_6$ (**9**)	2.923	0.222	2.053

Apparently, in the structures with ligand **4b** (**8** and **9**), which has the two "lateral" pyridyl substituents each tethered to the ligand core by an ethylene group (as opposed to methylene groups in **4a**), the bonds in the equatorial plane are longer overall, and this causes less repulsion for the d orbitals than in the structures with ligand **4a** (complexes **6** and **7**). This change in ligand-field strength alters the orbital energies, and this in turn leads to different transition energies, and hence a sign change for the *D* parameter.

Table 5. Different contributions to computed ZFS parameters for **6**–**9**.

Complex/parameter	**6**	**7**	**8**	**9**
D_{soc}	–1.831	–0.558	2.354	2.629
D_{ss}	–0.443	–0.468	0.231	0.291
SOMO–VMO[a] α→α	–0.225	0.056	0.654	0.746
DOMO–SOMO β→β	–0.480	–0.312	0.898	0.991
SOMO–SOMO α→β	–1.131	–0.309	0.752	0.842
DOMO–VMO β→α	0.005	0.007	0.050	0.05

[a] VMO: virtual molecular orbital.

The spin-density plot for **8** is shown in part d of Figure 4. A spin-density value of 3.753 has been found on the Fe^{II} atom, which indicates a slight delocalization of the unpaired spins to other coordinated atoms. Each of the coordinated nitrogen atoms have spin densities of ca. 0.02–0.03, whereas the chlorine atom has a much larger value of 0.09. For the iron ion in **6**, a spin density of 3.714 was detected and this is significantly less compared to that of **8**. As the average metal-to-ligand bond length is shorter in **6** (Table 3), greater delocalization takes places compared to that in **8** and **9**. The spin density distribution nicely reflects the orbital analysis described earlier. Complex **9** shows a similar spin distribution pattern, and the bromine atom gains a spin density of ca. 0.1 from the Fe^{II} centre.

Conclusion

The two pentadentate nitrogen ligands presented in this study, **4a** and **4b**, together with a chlorido or bromido ligand, give iron(II) complexes of the type [FeLX]$^+$, the coordination geometries of which differ markedly in their degrees of distortion from octahedral. The N_5 donor set of ligand **4a**, which has the two "lateral" pyridyl substituents each tethered to the ligand core by a single methylene group, is stereochemically more constricted than in the case of **4b**, in which the tethers each contain two methylene groups. Magnetic susceptibility measurements show all complexes to be paramagnetic in the temperature range $2 < T < 300$ K and to contain high-spin iron(II). DFT calculations have been performed on **6**–**9** to elucidate their electronic structures and to analyze the absence of SCO in this type of complex. Calculations reveal that a stronger ligand field exerted by the axial halogen ligand leads to a large d orbital splitting and a greater HS–LS gap. Further, this work nicely illustrates how a small modification in the chelate ligand can alter the sign of the ZFS parameter. The origin of the change in the sign of ZFS is rationalized by using computed results.

Experimental Section

General: Unless noted otherwise, all reactions were carried out in dry solvents under dry dinitrogen by using standard Schlenk techniques. Basic chemicals were purchased from Aldrich and used without further purification. IR spectra were measured as KBr disks. Spectroscopic data were obtained with the following instruments. IR spectroscopy: Nicolet MagnaSystem 750. NMR spectroscopy: Bruker ARX 200 and ARX 400. Elemental analyses were carried out with a Thermo Finnigan Flash EA 1112 series analyzer.

X-ray Crystallography: Data collection was performed at 150(1) K with an Oxford Diffraction Xcalibur S instrument equipped with a Sapphire3 CCD detector and graphite-monochromated Mo-K_α radiation with λ = 0.71073 Å from an Enhance X-ray source (Table 6). Frames were integrated by using the Scale3 Abspack algorithm.[38] The structures were solved by direct methods with the program SHELXS-97[39] (**7**–**9**) or by charge-flipping methods with Superflip[40] (**6**). Subsequent full-matrix least-squares refinement of F_o^2 data was carried out by using SHELXL-97.[39] All non-hydrogen atoms were refined anisotropically. Hydrogen atoms were located on Fourier difference maps and refined by using a riding model. The acetonitrile moieties in **8**·½MeCN and **9**·½MeCN are disordered over centres of inversion. In the former compound, it had to be treated with Platon/Squeeze,[41] whereas it could be refined with an occupancy of ½ on a single position in the latter. Molecular graphics were created with the software package ORTEP-3 for Windows.[42]

CCDC-902540 (for **6**·MeCN), -902539 (for **7**·MeCN), -902542 (for **8**·½ MeCN) and -902541 (for **9**·½ MeCN) contain the supplementary crystallographic data for this paper. These data can be obtained free of charge from The Cambridge Crystallographic Data Centre via http://www.ccdc.cam.ac.uk/data_request/cif.

Magnetic susceptibility data were collected with a Quantum Design MPMS 5 superconducting quantum interference device (SQUID) magnetometer under an applied field of 1 T. The samples were placed in a gel capsule, which was secured within a plastic straw that was attached to the sample rod. Care was taken to allow adequate thermal equilibration times at each temperature point. To achieve this, the change between temperatures (either cooling or heating) was at a rate of 10 K per minute, and the temperature was stabilized at particular temperatures between 2 and 70 K for 2 min and between 70 and 400 K for 5 min. The stabilization times were varied to find these aforementioned optimum times such that the magnetizations did not change. To avoid crystallite torquing for these potentially anisotropic high-spin Fe^{II} compounds, the samples were contained in Vaseline gel.[22]

Computational Details: All calculations were performed by using the hybrid B3LYP[43] functional with the Ahlrichs triple-ζ basis set[44,45] as implemented in the Gaussian 09 suite of programs.[46]

Calculations of the g tensors and ZFS values of complexes was performed by using the Orca programme suite. The calculations for D tensors were based on the X-ray structures. The DFT calculations were carried out at hybrid B3LYP levels of theory. We have employed the unrestricted Kohn–Sham formalism (UKS) for estimating D_{SS}. The calculations employed the resolution of identity (RI-J) algorithm for the computation of the Coulomb terms. In our DFT calculations, the spin–orbit coupling operators are represented by an effective one electron with the spin–orbit mean field (SOMF) method, which is implemented in Orca.[47] We have used the coupled perturbed SOC approach (CP) rather than the Pederson–Khanna (PK) approach to evaluate D_{SOC}. The spin–spin contribution (DSS) was estimated by using the unrestricted natural orbital (UNO) approach rather than the UKS approach. The spin–

Table 6. Crystallographic data for **6**–**9**.

	6·MeCN	**7**·MeCN	**8**·½ MeCN	**9**·½ MeCN
Empirical formula	$C_{25}H_{30}ClF_6FeN_6P$	$C_{25}H_{30}BrF_6FeN_6P$	$C_{26}H_{32.5}ClF_6FeN_{5.5}P$	$C_{26}H_{32.5}BrF_6FeN_{5.5}P$
M [g mol^{-1}]	650.82	695.28	658.34	702.80
Crystal dimensions [mm]	0.05 × 0.07 × 0.20	0.06 × 0.14 × 0.17	0.05 × 0.14 × 0.33	0.12 × 0.15 × 0.16
Crystal description	pale yellow prism	pale yellow plate	pale yellow plate	pale yellow spar
Crystal system	monoclinic	monoclinic	triclinic	triclinic
Space group	$P2_1/c$ (No. 14)	$P2_1/c$ (No. 14)	$P\bar{1}$ (No. 2)	$P\bar{1}$ (No. 2)
a [Å]	16.8407(5)	16.9098(7)	8.4201(4)	8.5704(7)
b [Å]	8.3178(2)	8.4160(3)	12.6853(7)	12.7299(10)
c [Å]	24.6954(9)	24.5552(12)	13.7091(8)	13.5549(11)
α [°]	90	90	92.301(5)	87.977(6)
β [°]	125.427(2)	125.173(3)	90.059(4)	89.472(7)
γ [°]	90	90	96.401(4)	83.927(7)
V [Å^3]	2818.80(15)	2856.5(2)	1453.97(14)	1469.6(2)
Z	4	4	2	2
ρ_{calc} [g cm^{-3}]	1.534	1.617	1.504	1.588
μ [mm^{-1}]	0.754	2.049	0.731	1.992
F(000)	1336	1408	678	714
T_{min}/T_{max}	0.82089/1.00000	0.83308/1.00000	0.80353/1.00000	0.78187/1.00000
$\theta_{min}/\theta_{max}$ [°]	3.31/26.00	3.37/26.00	3.38/26.00	3.35/26.00
Measured reflections	21417	12824	11071	11650
Independent reflections/R_{int}	5518/0.0403	5610/0.0500	5713/0.0278	5771/0.0398
Observed reflections/R_σ	4809/0.0398	4306/0.0742	4781/0.0424	4853/0.0553
Data/restraints/parameters	5518/0/363	5610/0/363	5711/0/353	5771/0/381
R_1 (observed/all data)	0.0383/0.0486	0.0480/0.0709	0.0417/0.0562	0.0499/0.0624
wR_2 (observed/refined)[a]	0.0791/0.0831	0.0843/0.0952	0.1042/0.1092	0.1135/0.1198
GoF	1.093	1.034	1.057	1.105
Residual density [e Å^{-3}]	–0.302/0.300	–0.664/0.704	–0.277/0.480	–0.537/1.035

[a] $wR_2 = [\Sigma w(F_o^2 - F_c^2)^2/\Sigma wF_o^4]^{1/2}$, $w = [\sigma^2(F_o^2) + (uP)^2 + vP] - 1$ with $P = [\max(F_o^2,0) + 2F_c^2]/3$.

orbit contributions were estimated by using the DKH method implemented in Orca.[47]

Syntheses: The numbering schemes used for the NMR assignments of **2**, **3** and **4a/b** are given in the Supporting Information.

6-Methyl-6-(pyridin-2-yl)-1,4-ditosyl-1,4-diazepane (2): Ethylenediamine-1,2-ditoslylate (15.7 mmol, 5.83 g) and NaOH (36.3 mmol, 1.45 g) were dissolved in H_2O (100 mL) and the mixture was heated to reflux until a clear solution had formed. After addition of a warm solution of 2-methyl-2-(pyridin-2-yl)propane-1,3-diyl bis(4-methylbenzenesulfonate) (15.7 mmol, 7.52 g) in toluene (100 mL), the emulsion was heated to reflux for 2 d. Subsequently, the warm (not boiling) organic phase was decanted, and the aqueous phase was washed with warm toluene (100 mL). Removal of toluene from the combined organic phases left the crude product as an orange solid, which was dissolved in $CHCl_3$. The insoluble components were removed by filtration, and the solvent of the filtrate was removed under reduced pressure to give **2** as an orange resinous solid. The product was used in subsequent syntheses without further purification; yield 6.80 g (86%). ^{1}H NMR (200 MHz, $CDCl_3$, 25 °C): δ = 8.54 (dm, $^3J_{H,H}$ = 4 Hz, 1 H, 11-H), 7.77–7.60 (m, 5 H, 13-H, 19-H, 23-H, 29-H, 33-H), 7.52 (d, $^3J_{H,H}$ = 8 Hz, 1 H, 14-H), 7.30–7.16 (m, 5 H, 12-H, 20-H, 22-H, 30-H, 32-H), 3.77 (d, $^2J_{H,H}$ = 14 Hz, 2 H, 5-H, 7-H), 3.61–3.44 (m, 4 H, 2-H, 3-H, 5-H, 7-H), 3.24–3.11 (m, 2 H, 2-H, 3-H), 2.41 (s, 6 H, 24-H, 34-H), 1.56 (s, 3 H, 8-H) ppm. {^{1}H}^{13}C NMR (50.32 MHz, $CDCl_3$, 25 °C): δ = 163.19 (1 C, C-9), 148.26 (1 C, C-11), 143.73 (2 C, C-21, C-31), 137.31 (1 C, C-13), 135.50 (2 C, C-18, C-28), 129.96 (4 C, C-20, C-22, C-30, C-32), 127.32 (4 C, C-19, C-23, C-29, C-33), 122.13 (1 C, C-14), 121.35 (1 C, C-12), 58.17 (2 C, C-2, C-3), 51.23 (2 C, C-5, C-7), 46.10 (1 C, C-6), 23.98 (1 C, C-8), 21.62 (2 C, C-24, C-34) ppm. HRMS (ESI): calcd. for $C_{25}H_{29}N_3O_4S_2$ [M + H]$^+$ 500.1672; found 500.1666.

6-Methyl-6-(pyridin-2-yl)-1,4-diazepane (3): Compound **2** (10.0 mmol, 5.00 g) was dissolved in H_2SO_4 (20 mL). The reaction mixture was heated to 130 °C for 14 h, after which time a black suspension had formed. The mixture was cooled to 0 °C and carefully basified with saturated aqueous NaOH. The aqueous solution was extracted three times with $CHCl_3$. The volatiles were then removed from the combined organic phases with a rotary evaporator to leave a yellow oil. The product was used in subsequent syntheses without purification; yield 1.59 g (80%). ^{1}H NMR (200 MHz, $CDCl_3$, 25 °C): δ = 8.55 (dm, $^3J_{H,H}$ = 4 Hz, 1 H, 11-H), 7.63 (td, $^3J_{H,H}$ = 8, $^4J_{H,H}$ = 2 Hz, 1 H, 13-H), 7.34 (d, $^3J_{H,H}$ = 8 Hz, 1 H, 14-H), 7.15–7.08 (m, 1 H, 12-H), 3.41 (d, $^2J_{H,H}$ = 14 Hz, 2 H, 5-H, 7-H), 2.96 (s, 4 H, 2-H, 3-H), 2.87 (d, $^2J_{H,H}$ = 14 Hz, 2 H, 5-H, 7-H), 2.36 (br. s, 2 H, 1-H, 4-H), 1.25 (s, 3 H, 8-H) ppm. {^{1}H}^{13}C NMR (50.32 MHz, $CDCl_3$, 25 °C): δ = 167.04 (1 C, C-9), 148.90 (1 C, C-11), 136.64 (1 C, C-13), 121.31 (1 C, C-14), 120.49 (1 C, C-12), 60.20 (2 C, C-2, C-3), 52.58 (2 C, C-5,C-7), 47.47 (1 C, C-6), 24.93 (1 C, C-8) ppm. HRMS (ESI): calcd. for $C_{11}H_{17}N_3$ [M + H]$^+$ 192.1495; found 192.1490.

6-Methyl-6-(pyridin-2-yl)-1,4-bis[(pyridin-2-yl)methyl]-1,4-diazepane (4a): Solid K_2CO_3 (59.04 mmol, 8.16 g) and 2-picolyl chloride hydrochloride (11.81 mmol, 1.94 g) were added to a solution of **3** (5.91 mmol, 1.13 g) in MeCN (70 mL, no care was taken to exclude moisture from the solvent.) The resulting suspension was stirred at 55 °C for 3 d. and was then allowed to cool to room temperature. The solvent was removed with a rotary evaporator, and the residue dissolved in toluene (30 mL). Crude **4a** was obtained as an orange oil after washing the toluene phase with water and the subsequent removal of the solvent under reduced pressure. Trituration of the crude product with hexane and removal of the solvent with a rotary evaporator yielded the product as a clear orange oil; yield 2.01 g (91%). ^{1}H NMR (200 MHz, $CDCl_3$, 25 °C): δ = 8.48–8.42 (m, 3 H, 11-H, 18-H, 25-H), 7.61–7.34 (m, 6 H, 13-H, 14-H, 20-H, 21-H, 27-H, 28-H), 7.13–6.99 (m, 3 H, 12-H, 19-H, 26-H), 3.85 (br. s, 4 H, 15-H, 22-H), 3.39 (d, 2 H, 5-H, 7-H), 2.92–2.72 (m, 6 H, 2-H, 3-H, 5-H, 7-H), 1.21 (s, 3 H, 8-H) ppm. {^{1}H}^{13}C NMR (50.32 MHz, $CDCl_3$, 25 °C): δ = 167.46 (1 C, C-9), 159.99 (2 C, C-16, C-23), 148.94 (2C, C-18, C-25), 148.33 (1C, C-11), 136.39 (2 C, C-20, C-27), 136.04 (1 C, C-13), 123.25 (2 C, C-21, C-28), 122.01 (1 C, C-14), 121.02 (2 C, C-19, C-26), 120.92 (1 C, C-12), 67.29 (2 C, C-5, C-7), 66.27 (2 C, C-15, C-22), 59.25 (2 C, C-2, C-3), 46.04 (1 C, C-6), 25.64 (1 C, C-8) ppm. $C_{23}H_{27}N_5$ (373.49): calcd. C 73.96, H 7.29, N 18.75; found C 73.20, H 7.26, N 18.88. HRMS (ESI): calcd. for $C_{23}H_{27}N_5$ [M + H]$^+$ 374.2339; found 374.2331.

6-Methyl-6-(pyridin-2-yl)-1,4-bis[2-(pyridin-2-yl)ethyl]-1,4-diazepane (4b): To a solution of **3** (5.8 mmol, 1.10 g) in MeOH (30 mL) was added acetic acid (14.4 mmol, 0.86 g) and 2-vinylpyridine (28.8 mmol, 3.02 g). The reaction mixture was warmed to 65 °C and stirred for 2 d. The mixture was then cooled to room temperature, and the volatiles were removed under reduced pressure. The remaining red-brown oil was dissolved in H_2O and carefully made basic with solid NaOH. Compound **4b** was subsequently extracted three times with toluene. The removal of toluene from the combined organic phases left the crude product as a red oil, which was purified by repeated extraction with small amounts of hexane. The solvent was removed in vacuo to give **4b** as a light yellow oil; yield 1.42 g (61%). ^{1}H NMR (200 MHz, $CDCl_3$, 25 °C): δ = 8.50 (dm, $^3J_{H,H}$ = 4 Hz, 3 H, 11-H), 7.58–7.46 (m, 3 H, 13-H, 21-H, 29-H), 7.36 (d, $^3J_{H,H}$ = 8 Hz, 1 H, 14-H), 7.12–7.04 (m, 5 H, 22-H, 30-H, 12-H, 20-H, 28-H), 3.17 (d, $^2J_{H,H}$ = 14 Hz, 2 H, 5-H, 7-H), 2.91 (br. s, 8 H, 2-H, 3-H, 15-H, 23-H), 2.81–2.68 (m, 6 H, 5-H, 7-H, 16-H, 24-H), 1.23 (s, 3 H, 8-H) ppm. {^{1}H}^{13}C NMR (50.32 MHz, $CDCl_3$, 25 °C): δ = 167.81 (1 C, C-9), 160.94 (2 C, C-17, C-25), 149.34 (2 C, C-19, C-27), 148.35 (1 C, C-11), 136.24 (2 C, C-21, C-29), 136.02 (1 C, C-13), 123.48 (2 C, C-22, C-30), 121.29 (1 C, C-14), 121.10 (2 C, C-20, C-28), 120.95 (1 C, C-12), 67.11 (2 C, C-5, C-7), 60.67 (2 C, C-2, C-3), 59.56 (2 C, C-15, C-23), 45.70 (1 C, C-6), 36.30 (2 C, C-16, C-24), 25.35 (1 C, C-8) ppm. $C_{25}H_{31}N_5$ (401.55): calcd. C 74.78, H 7.78, N 17.44; found C 74.73, H 7.92, N 17.29. HRMS (ESI): calcd. for $C_{25}H_{31}N_5$ [M + H]$^+$ 402.2652; found 402.2634.

[Fe(4b)Br]Br (5): A solution of $FeBr_2$ (0.74 mmol, 0.16 mg) in MeOH (3 mL) was added to a methanolic solution (3 mL) of **4b** (0.78 mmol, 0.31 mg). The solution was left to stir at room temperature overnight before the volume of the solution was reduced to ca. 1 mL with an oil-pump vacuum. The addition of Et_2O (15 mL) precipitated **5** as a yellow powder. The suspension was centrifuged, the organic solvent was decanted, and the yellow solid was washed with Et_2O (2 × 10 mL) and dried in vacuo; yield 0.39 g (81%). $C_{25}H_{31}Br_2FeN_5$ (617.20): calcd. C 48.65, H 5.06, N 11.35; found C 49.19, H 5.18, N 11.31. HRMS (ESI): calcd. for $C_{25}H_{31}BrFeN_5$ [M]$^+$ 536.1107; found 536.1096; calcd. for $C_{25}H_{31}FeN_5$ [M]$^{2+}$ 228.5959; found 228.5956.

[Fe(4a)Cl](PF$_6$) (6): A solution of $FeCl_2$ (0.42 mmol, 0.05 g) in MeOH (2 mL) was added to a solution of **4a** (0.44 mmol, 0.17 g) in MeOH (2 mL), and the mixture was stirred for 1 h at room temperature. The addition of solid (nBu$_4$N)PF$_6$ produced a yellow precipitate, which was removed by filtration and washed with Et_2O. Isothermal diffusion of Et_2O into a solution of the yellow solid in MeCN generated crystals of **6**. The crystals were washed with Et_2O and dried in vacuo to give a product with the correct elemental analysis; yield 0.22 g (84%). $C_{23}H_{27}ClF_6FeN_5P$ (609.76): calcd. C

45.30, H 4.46, N 11.49; found C 45.30, H 4.31, N 11.13. HRMS (ESI): calcd. for $C_{23}H_{27}ClFeN_5$ $[M]^+$ 464.1299; found 464.1288; calcd. for $C_{25}H_{27}FeN_5$ $[M]^{2+}$ 214.5802; found 214.5798.

[Fe(4a)Br](PF$_6$)·MeCN (7): A solution of $FeBr_2$ (0.33 mmol, 0.07 g) in MeOH (3 mL) was added to a solution of **4a** (0.35 mmol, 130 mg) in MeOH to give a yellow solution, which was stirred for 12 h at room temperature. The addition of solid (nBu$_4$N)PF$_6$ (0.66 mmol, 0.23 g) caused the precipitation of a yellow solid. The suspension was stirred for an additional 12 h at room temperature, and the yellow precipitate was collected by filtration, washed with Et_2O and dissolved in MeCN. The isothermal diffusion of Et_2O into this solution produced **7** as a yellow crystalline material, which was collected by filtration and dried in vacuo; yield 0.18 g, 79%. $C_{25}H_{30}BrF_6FeN_6P$ (695.26): calcd. C 43.19, H 4.35, N 12.09; found C 43.80, H 4.56, N 11.90. HRMS (ESI): calcd. for $C_{23}H_{27}BrFeN_5$ $[M]^+$ 508.0794; found 508.0782; calcd. for $C_{23}H_{27}FeN_5$ $[M]^{2+}$ 214.5802; found 214.5798.

[Fe(4b)Cl](PF$_6$) (8): $FeCl_2$ (0.24 mmol, 0.03 g) and **4b** (0.25 mmol, 0.10 g) were dissolved in MeOH (3 mL), and the mixture was stirred at room temperature for 4 h. The addition of solid (nBu$_4$N)-PF$_6$ (0.47 mmol, 0.18 g) precipitated the product as a yellow solid. The material was collected by filtration, washed with Et_2O and dissolved in MeCN. The thermal diffusion of Et_2O into this solution generated **8** as a yellow crystalline solid, which was collected by filtration, washed with Et_2O and dried in vacuo; yield 0.07 g (44%). $C_{25}H_{31}ClF_6FeN_5P$ (637.81): calcd. C 47.08, H 4.90, N 10.98; found C 47.56, H 5.01, N 10.73. HRMS (ESI): calcd. for $C_{25}H_{31}BrFeN_5$ $[M]^+$ 536.1107; found 536.1096; calcd. for $C_{25}H_{31}FeN_5$ $[M]^{2+}$ 228.5959; found 228.5956.

[Fe(4b)Br](PF$_6$) (9): Solid (nBu$_4$N)PF$_6$ (0.4 mmol, 0.15 g) was added to a stirred solution of **5** (0.3 mmol, 0.20 g) in MeOH (4 mL). After a few seconds, a yellow solid started to precipitate, and stirring of the suspension was continued overnight. Compound **9** was collected by filtration, washed with Et_2O and dried under reduced pressure; yield 0.14 g (63%). Yellow single crystals of **9** formed in a solution of the complex in MeCN after 5 d upon isothermal diffusion of Et_2O. $C_{25}H_{31}BrF_6FeN_5P$ (682.26): calcd. C 44.01, H 4.58, N 10.26; found C 43.85, H 4.74, N 9.92. HRMS (ESI): calcd. for $C_{25}H_{31}BrFeN_5$ $[M]^+$ 536.1107; found 536.1096; calcd. for $C_{25}H_{31}FeN_5$ $[M]^{2+}$ 228.5959; found 228.5956.

Supporting Information (see footnote on the first page of this article): $\chi_M T$ vs. T for **7** and **9**. Numbering scheme for NMR assignments.

Acknowledgments

One of the authors (A. G.) gratefully acknowledges support of this work by the Deutsche Forschungsgemeinschaft (DFG) (grant number GR 1247/7-1; SFB 658: *Elementary Processes in Molecular Switches on Surfaces*). K. S. M. acknowledges financial support through a Discovery Grant by the Australian Research Council (ARC). G. R. and K. S. M. acknowledge support by the Australia-India Strategic Research Fund (AISRF); Department of Innovation, Industry, Science and Research, Canberra (Project: New Generation Molecular Magnetic Materials: Experiment and Theory; DST/INT/AUS/P-47/11). K. R. V. is thankful to the IITB-Monash Academy for a PhD studentship.

[1] B. Kräutler, B. Jaun, in: *Concepts and Models in Bioinorganic Chemistry* (Eds.: H.-B. Kraatz, N. Metzler-Nolte), Wiley-VCH, Weinheim, Germany, **2006**, p. 177.
[2] T. A. Jackson, L. Que Jr., in: *Concepts and Models in Bioinorganic Chemistry* (Eds.: H.-B. Kraatz, N. Metzler-Nolte), Wiley-VCH, Weinheim, Germany, **2006**, p. 259.
[3] P. Gütlich, H. A. Goodwin, *Top. Curr. Chem.* **2004**, *233*, 1–47.
[4] *Spin-crossover materials - properties and applications* (Ed.: M. A. Halcrow), John Wiley & Sons, Chichester, UK, **2012**, in press.
[5] A. Grohmann, *Dalton Trans.* **2010**, *39*, 1432–1440.
[6] J. Pitarch López, H. Kämpf, M. Grunert, P. Gütlich, F. W. Heinemann, R. Prakash, A. Grohmann, *Chem. Commun.* **2006**, 1718–1720.
[7] J. Pitarch López, F. W. Heinemann, R. Prakash, B. A. Hess, O. Horner, C. Jeandey, J.-L. Oddou, J.-M. Latour, A. Grohmann, *Chem. Eur. J.* **2002**, *8*, 5709–5722.
[8] P. Comba, W. Schiek, *Coord. Chem. Rev.* **2003**, *238–239*, 21–29.
[9] M. Schmidt, D. Wiedemann, A. Grohmann, *Inorg. Chim. Acta* **2011**, *374*, 514–520.
[10] S. Friedrich, M. Schubart, L. H. Gade, I. L. Scowen, J. Andrew, M. McPartlin, *Chem. Ber./Recueil* **1997**, *130*, 1751–1759.
[11] J. Romba, D. Kuppert, B. Morgenstern, C. Neis, S. Steinhauser, T. Weyhermüller, K. Hegetschweiler, *Eur. J. Inorg. Chem.* **2006**, 314–328.
[12] H. Chong, K. Garmestani, D. Ma, D. E. Milenic, T. Overstreet, M. W. Brechbiel, *Med. J. Chem.* **2002**, *45*, 3458–3464.
[13] C. He, S. J. Lippard, *Tetrahedron* **2000**, *56*, 8245–8252.
[14] I. Blain, M. Giorgi, I. de Riggi, M. Réglier, *Eur. J. Inorg. Chem.* **2000**, 393–398.
[15] N. Ortega-Villar, V. M. Ugalde-Saldívar, M. C. Muñoz, L. A. Ortiz-Frade, J. G. Alvarado-Rodríguez, J. A. Real, R. Moreno-Esparza, *Inorg. Chem.* **2007**, *46*, 7285–7293.
[16] M. Haryono, F. W. Heinemann, K. Petukhov, K. Gieb, P. Müller, A. Grohmann, *Eur. J. Inorg. Chem.* **2009**, 2136–2143.
[17] H. Zabrodsky, S. Peleg, D. Avnir, *J. Am. Chem. Soc.* **1992**, *114*, 7843–7851.
[18] Calculations were performed by using the online service of the Hebrew University of Jerusalem, see: A. Zayit, M. Pinsky, H. Elgavi, C. Dryzun, D. Avnir, *Chirality* **2011**, *23*, 17–23.
[19] P. Guionneau, M. Marchivie, G. Bravic, J.-F. Létard, D. Chasseau, *J. Mater. Chem.* **2002**, *12*, 2546–2551.
[20] N. F. Chilton, R. P. Anderson, L. D. Turner, A. Soncini, K. S. Murray, *J. Comput. Chem.* **2013**, in press.
[21] P. Gütlich, E. Bill, A. X. Trautwein, *Mössbauer Spectroscopy and Transition Metal Chemistry: Fundamentals and Applications*, Springer-Verlag, Berlin, **2011**.
[22] B. J. Kennedy, K. S. Murray, *Inorg. Chem.* **1985**, *24*, 1552–1557.
[23] D. E. Freedman, W. H. Harman, T. D. Harris, G. J. Long, C. J. Chang, J. R. Long, *J. Am. Chem. Soc.* **2010**, *132*, 1224–1225.
[24] E. Cremades, E. Ruiz, *Inorg. Chem.* **2011**, *50*, 4016–4020.
[25] F. Neese, *Coord. Chem. Rev.* **2009**, *253*, 526–563.
[26] S. Ye, F. Neese, *Inorg. Chem.* **2010**, *49*, 772–774.
[27] C. R. Jacob, M. Reiher, *Int. J. Quantum Chem.* **2012**, *112*, 3661–3684.
[28] K. P. Kepp, *Coord. Chem. Rev.* **2013**, 257, 196.
[29] E. König, *Struct. Bonding (Berlin)* **1991**, *76*, 51–152.
[30] J. M. Holland, J. A. McAllister, Z. Lu, C. A. Kilner, M. Thornton-Pett, M. A. Halcrow, *Chem. Commun.* **2001**, 577–578.
[31] P. Gütlich, H. A. Goodwin, *Top. Curr. Chem.* **2004**, *233*, 13–14.
[32] A recent example in which the exchange of a halido for a thiocyanato ligand leads to a complex showing temperature-dependent spin crossover is: M. Bernien, D. Wiedemann, C. F. Hermanns, A. Krüger, D. Rolf, W. Kroener, P. Müller, A. Grohmann, W. Kuch, *J. Phys. Chem. Lett.* **2012**, *3*, 3431–3434.
[33] K. S. Murray, C. J. Kepert, *Top. Curr. Chem.* **2004**, *233*, 195–228.
[34] S. Schlamp, P. Thoma, B. Weber, *Eur. J. Inorg. Chem.* **2012**, 2759–2768.
[35] E. Cremades, E. Ruiz, *Inorg. Chem.* **2011**, *50*, 4016–4020.

[36] F. Neese, *J. Am. Chem. Soc.* **2006**, *128*, 10213–10222.
[37] N. Berg, T. N. Hooper, J. Liu, C. C. Beedle, S. K. Singh, G. Rajaraman, S. Piligkos, S. Hill, E. K. Brechin, L. F. Jones, *Dalton Trans.* **2013**, *42*, 207–216.
[38] *CrysAlisPro Software System, Intelligent Data Collection and Processing Software for Small Molecule and Protein Crystallography*, Agilent Technologies, Ltd., Oxford, UK, **2011**.
[39] G. M. Sheldrick, *Acta Crystallogr., Sect. A: Found. Crystallogr.* **2008**, *64*, 112–122.
[40] L. Palatinus, G. Chapuis, *J. Appl. Crystallogr.* **2007**, *40*, 786–790.
[41] P. van der Sluis, A. L. Spek, *Acta Crystallogr., Sect. A: Found. Crystallogr.* **1990**, *46*, 194–201.
[42] L. J. Farrugia, *J. Appl. Crystallogr.* **1997**, *30*, 565.
[43] A. D. Becke, *J. Chem. Phys.* **1993**, *98*, 5648–5652.
[44] A. Schäfer, H. Horn, R. Ahlrichs, *J. Chem. Phys.* **1992**, *97*, 2571–2577.
[45] A. Schäfer, C. Huber, R. Ahlrichs, *J. Chem. Phys.* **1994**, *100*, 5829–5835.
[46] M. J. Frisch, G. W. Trucks, H. B. Schlegel, G. E. Scuseria, M. A. Robb, J. R. Cheeseman, G. Scalmani, V. Barone, B. Mennucci, G. A. Petersson, H. Nakatsuji, M. Caricato, X. Li, H. P. Hratchian, A. F. Izmaylov, J. Bloino, G. Zheng, J. L. Sonnenberg, M. Hada, M. Ehara, K. Toyota, R. Fukuda, J. Hasegawa, M. Ishida, T. Nakajima, Y. Honda, O. Kitao, H. Nakai, T. Vreven, J. A. Montgomery Jr., J. E. Peralta, F. Ogliaro, M. Bearpark, J. J. Heyd, E. Brothers, K. N. Kudin, V. N. Staroverov, R. Kobayashi, J. Normand, K. Raghavachari, A. Rendell, J. C. Burant, S. S. Iyengar, J. Tomasi, M. Cossi, N. Rega, J. M. Millam, M. Klene, J. E. Knox, J. B. Cross, V. Bakken, C. Adamo, J. Jaramillo, R. Gomperts, R. E. Stratmann, O. Yazyev, A. J. Austin, R. Cammi, C. Pomelli, J. W. Ochterski, R. L. Martin, K. Morokuma, V. G. Zakrzewski, G. A. Voth, P. Salvador, J. J. Dannenberg, S. Dapprich, A. D. Daniels, O. Farkas, J. B. Foresman, J. V. Ortiz, J. Cioslowski, D. J. Fox, *Gaussian 09*, rev. A.02, Gaussian, Inc., Wallingford CT, **2009**.
[47] F. Neese, *Orca*, v. 2.9-35, *An ab initio, DFT and Semiempirical SCF-MO Package*, Max-Planck-Institut für Chemische Energiekonversion, Mülheim an der Ruhr, Germany, **2012**.

Received: September 25, 2012
Published Online: January 18, 2013

